Cell, Vol. 89, 425–435, May 2, 1997, Copyright ©1997 by Cell Press

Defective Transcription-Coupled Repair in Cockayne Syndrome B Mice Is Associated with Skin Cancer Predisposition

Gijsbertus T. J. van der Horst,* Harry van Steeg,† Rob J. W. Berg,‡ Alain J. van Gool,* Jan de Wit,* Geert Weeda,* Hans Morreau,§ Rudolf B. Beems,† Coen F. van Kreijl,† Frank R. de Gruijl,‡ Dirk Bootsma,* and Jan H. J. Hoeijmakers*
*Medical Genetics Center
Department of Cell Biology and Genetics
Erasmus University Rotterdam
P.O. Box 1738
3000 DR Rotterdam
The Netherlands
†Department of Carcinogenesis, Mutagenesis and Genetics
National Institute of Public Health and Environmental Protection
3720 BA Bilthoven
The Netherlands
‡Department of Dermatology
University of Utrecht
3584 CX Utrecht
The Netherlands
§Department of Pathology
Leiden University Hospital
2300 RL Leiden
The Netherlands

Summary

A mouse model for the nucleotide excision repair disorder Cockayne syndrome (CS) was generated by mimicking a truncation in the *CSB(ERCC6)* gene of a CS-B patient. CSB-deficient mice exhibit all of the CS repair characteristics: ultraviolet (UV) sensitivity, inactivation of transcription-coupled repair, unaffected global genome repair, and inability to resume RNA synthesis after UV exposure. Other CS features thought to involve the functioning of basal transcription/repair factor TFIIH, such as growth failure and neurologic dysfunction, are present in mild form. In contrast to the human syndrome, CSB-deficient mice show increased susceptibility to skin cancer. Our results demonstrate that transcription-coupled repair of UV-induced cyclobutane pyrimidine dimers contributes to the prevention of carcinogenesis in mice. Further, they suggest that the lack of cancer predisposition in CS patients is attributable to a global genome repair process that in humans is more effective than in rodents.

Introduction

Maintenance of genetic information is of vital importance to living organisms. Damage to DNA can lead to mutations that are the cause of inborn defects, cell death, or cellular dysfunction, including escape from control of growth. To counteract the deleterious effects of environmental and endogenous genotoxic agents, all organisms have developed a complex network of repair systems that keeps the DNA under continuous surveillance (reviewed by Friedberg et al., 1995). A universal repair pathway dealing with a very wide spectrum of lesions is the nucleotide excision repair (NER) system. The range of structurally unrelated DNA damage eliminated by this process varies from ultraviolet (UV)–induced cyclobutane pyrimidine dimers (CPDs) and pyrimidine (6–4) pyrimidone photoproducts to numerous chemical adducts and intrastrand crosslinks.

In humans, inherited defects in NER are associated with at least three distinct photosensitive disorders: xeroderma pigmentosum (XP), Cockayne syndrome (CS), and trichothiodystrophy (TTD). Complementation studies with patient cell lines have revealed the existence of seven genes in XP (*XPA* through *XPG*), two in CS (*CSA* and *CSB*), and three in TTD (*TTDA*, *XPB*, and *XPD*). Analysis of cloned NER genes and the development of in vitro reconstitution systems with purified proteins (Aboussekhra et al., 1995) have recently culminated in the contours of a model for the NER reaction (reviewed by Hoeijmakers, 1994; Friedberg et al., 1995; Wood, 1996). NER is a complex process involving the concerted action of approximately 30 proteins in sequential damage recognition, chromatin remodeling, incision of the damaged DNA strand on both sides of the lesion, excision of the 27–29–mer oligonucleotide containing the damage, and gap-filling DNA synthesis followed by strand ligation.

One of the immediate effects of DNA damage is blockage of transcription. To allow rapid resumption of this vital process, the NER system has developed a mechanism to direct DNA repair preferentially to the transcribed strand of active genes (called transcription-coupled repair [TCR]). This specialized subpathway of NER is an important backup system for the removal of lesions for which the global genome repair process is too slow, such as UV-induced CPDs (Bohr et al., 1985; Mellon et al., 1987; reviewed by Hanawalt, 1994). All XP and TTD complementation groups are deficient in global genome repair and, with the exception of XP group C, also deficient in TCR. A specific defect in TCR is encountered in CS (Venema et al., 1990; van Hoffen et al., 1993), which results from mutations in the *CSA* or *CSB* gene (Troelstra et al., 1992; Henning et al., 1995). Fibroblasts from CS patients, despite exhibiting normal global genome repair activity, are UV-sensitive and unable to recover RNA synthesis after UV exposure. The precise role of CSA and CSB in TCR still remains elusive. The CSB protein contains SWI2/SNF2-like DNA-dependent ATPase domains, implying a possible role in chromatin remodeling and/or clearance of DNA by displacement of a stalled RNA polymerase, permitting repair proteins access to the lesion (Troelstra et al., 1992; Hanawalt et al., 1994; Peterson, 1996). It also has been proposed that, alternatively, CSA and CSB act as repair–transcription uncoupling proteins for rechanneling basal transcription/repair factor TFIIH from a repair mode into a transcription mode (van Oosterwijk et al., 1996).

The clinical consequences of defective NER are apparent from the phenotypes of NER disorders. The uniform hallmark is a pronounced hypersensitivity to UV light. XP patients are affected by pigmentation anomalies and a dramatic 2000-fold elevated risk of skin cancer

in sun-exposed areas, often in combination with progressive neurological degeneration (Bootsma et al., 1996). Paradoxically, in CS, although the NER defect is limited to TCR and thus milder than in XP, the clinical features are more severe. Patients present with postnatal growth failure, impaired sexual development, and severe neurological dysfunction (resulting from neurodysmyelination), including mental retardation, disturbed gait, ocular abnormalities, and sensorineural hearing loss. CS patients also have photosensitive skin, but in contrast to XP patients, they have not been reported to develop skin cancer at an increased rate (Nance and Berry, 1992). Although CS and XP are very rare conditions, some XP patients have combined symptoms of CS and XP; their disorders are classified into XP groups B, D, and G. TTD, in addition to producing the symptoms observed in CS, results in ichthyosis and brittle hair and nails due to a reduction in the content of cysteine-rich matrix proteins (Itin and Pittelkow, 1990).

Several pertinent questions arise in relation to these conditions. First, how can three distinct disorders be associated with deficiencies in one process and, in the case of XP-B and XP-D, even with one gene? While the XP features can be interpreted in terms of a repair defect, it is difficult to rationalize most of the CS and TTD symptoms on this basis. Second, CS-A and CS-B patients display additional clinical features, although they have only part of the NER defect of XP individuals. Third, why are CS and TTD, despite their repair defect not associated with skin cancer? A clue to an answer to the first question came from the discovery that the three NER gene products linked with TTD (XPB, XPD, and TTDA) are all components of the basal transcription/repair factor TFIIH and thus have a dual function: DNA repair and basal transcription (Schaeffer et al., 1993, 1994; Vermeulen et al., 1994b). As a consequence, mutations in the *XPB* or *XPD* gene not only affect repair but also may influence basal transcription. According to the ''transcription syndrome'' concept (Bootsma and Hoeijmakers, 1993; Vermeulen et al., 1994b), the CS or TTD features in XPB and XPD deficiencies are derived from crippling of the transcription function of TFIIH, affecting expression of a specific set of genes. On the basis of the resemblance in clinical symptoms, it is inferred that mutations in *XPG* as well as in *CSA* and *CSB* must also affect the functioning of TFIIH in basal transcription (Hoeijmakers et al., 1996). However, the above ideas do not explain why CS and TTD, despite their NER defect, fail to exhibit the dramatic cancer predisposition associated with XP.

To understand the role of (defective) NER proteins in mutagenesis, carcinogenesis, and the onset of clinical symptoms, animal mutants for photosensitive disorders are indispensable. Recently, mouse models for XP-A and XP-C have been shown to reflect reliably the skin cancer predisposition of the corresponding human disorder but few of the other features (de Vries et al., 1995; Nakane et al., 1995; Sands et al., 1995). The important question on cancer predisposition and the issues on the etiology of the CS features can be addressed when an animal model for CS is available. The present study describes the generation and characterization of a mouse model for CS.

Results

Generation of a CSB-Deficient Mouse

Since disruption of the mouse *CSB* gene at a random position might exert unpredictable effects, we wished to closely mimic the $K_{337}\rightarrow$stop mutation (allele *a* in compound heterozygote CS-B patient CS1AN), which has been shown to be nonlethal at the cellular level (Troelstra et al., 1992). Vector pG7CSBko1 was constructed by the insertion of a dominant-selectable *neo* marker and a multiple reading frame insertion (MURFI) ochre stop codon linker in exon 5 (Figure 1A). This position of the premature translational stop corresponds closely with the human mutation (Figure 1B) and skips all functional parts and highly conserved domains in the CSB protein. Since the effect of insertion of the dominant marker in the *CSB* gene on transcription and mRNA processing is not known, *loxP* sites were included to allow removal of the marker if necessary.

Heterozygous embryonic stem (ES) cell lines carrying a mutated *CSB* allele were generated by transfection of pG7CSBko1 into E14 ES cells, G418 selection, and Southern blot analysis of 126 neomycin-resistant clones. Homologous recombination, detected using a probe external to the construct and verified using a *neo* probe and a probe internal to the construct, occurred at a frequency of 17%. All ES lines contained the ochre stop codon (diagnosed by the HpaI site) and lacked additional random integration of the construct (data not shown). After verification of the normal ($n = 40$) chromosome content and the absence of visible translocations, cells from two independent ES lines were injected into C57BL/6J blastocysts. The chimeric male mice obtained were mated with FVB females and produced heterozygous offspring. Subsequent crossing of heterozygous animals yielded homozygous mutant mice in Mendelian fashion (detailed genotyping is shown in Figure 1C). Moreover, the two independent mouse lines were biochemically and phenotypically indistinguishable, which excludes the possibility that random events influenced the phenotype.

Disruption of the *CSB* Gene Results in a CS1AN-Like Allele

The effect of targeted disruption on expression of the *CSB* gene was studied in cultured fibroblasts derived from mouse embryos of all three genotypes. Relative *CSB* mRNA levels were determined by reverse transcription polymerase chain reaction (RT-PCR) on poly(A)$^+$ RNA using primer set FP/RP. The predicted 664 bp wild-type and 674 bp mutant PCR fragments, differing only at the position of the ochre linker, could be distinguished by PstI digestion. As shown in Figure 2A, $CSB^{-/-}$ fibroblasts are positive for the PstI-resistant PCR product, indicating that the targeted allele is expressed at the RNA level. Assuming that the minimal difference in sequence and length does not influence the amplification efficiency of the two products, the ratio of PstI-resistant/sensitive fragments in $CSB^{+/-}$ fibroblasts is indicative of the relative expression level of mutant mRNA. We infer that the *CSB–neo* fusion transcript was present at about one third the level of wild-type *CSB* mRNA. In

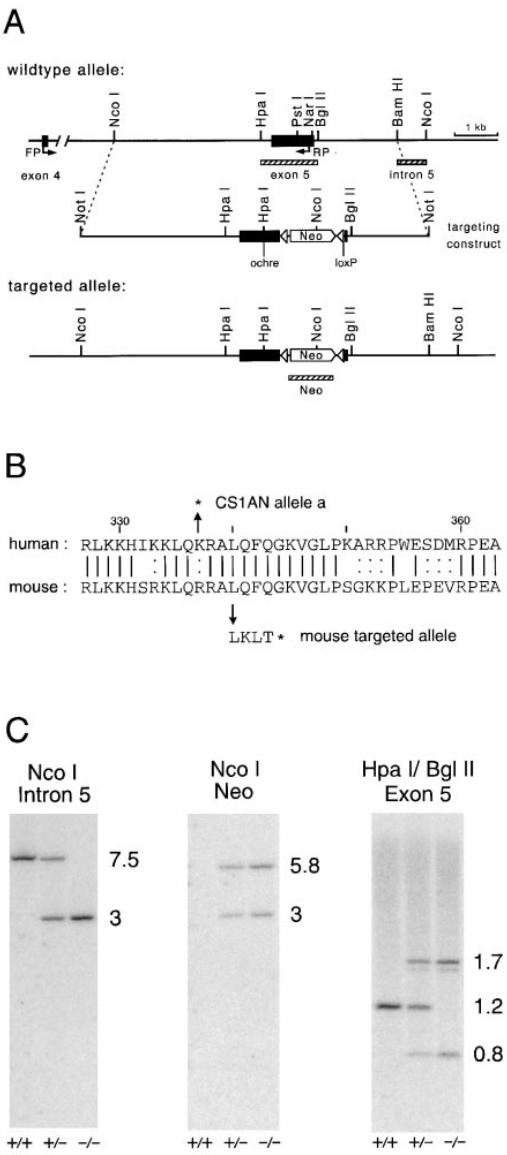

Figure 1. Targeting of the Mouse *CSB* Gene

(A) Schematic representation of the wild-type mouse *CSB* locus surrounding exon 5, the targeting construct (pG7CSBko1), and the targeted locus. Probes (intron 5, exon 5, and *neo*) and RT-PCR primers are indicated. Note the substitution of the PstI site for the HpaI site after insertion of the ochre MURFI linker.

(B) Partial amino acid sequence of exon 5 of the mouse and human *CSB* genes. The mutations in allele *a* of CS patient CS1AN and the targeted mouse allele are indicated. Introduction of the ochre MURFI linker changes L to LKLT* and causes a frameshift of the downstream sequence. Numbering is according to the human sequence.

(C) Southern blot analysis of tail DNA from $CSB^{+/+}$, $CSB^{+/-}$, and $CSB^{-/-}$ mice. For standard genotyping, NcoI-digested DNA was hybridized with the intron 5 probe. The wild-type and targeted alleles gave fragments of 7.5 and 3 kb, respectively. The absence of randomly integrated copies of the targeting construct was verified by hybridization of NcoI-digested DNA with the *neo* probe. The presence of the ochre stop codon in the targeted allele was confirmed by hybridization of HpaI/BglII-digested DNA with the exon 5 probe. Owing to the ochre MURFI linker–derived HpaI site and additional *neo* sequences, the 1.2 kb wild-type fragment was converted into fragments of 1.7 and 0.8 kb.

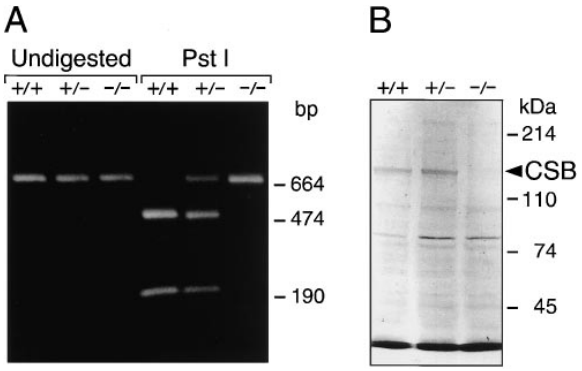

Figure 2. Expression of the Targeted *CSB* Allele

(A) RT-PCR analysis of purified mRNA from $CSB^{+/+}$, $CSB^{+/-}$, and $CSB^{-/-}$ mouse fibroblasts. Primer set FP/RP directs the amplification of 664 and 674 bp fragments from wild-type and fusion transcript–derived cDNA, respectively. Wild-type and mutant PCR fragments can be distinguished on the basis of the presence or absence, respectively, of a PstI restriction site (see Figure 1A).

(B) Western blot analysis of CSB protein in cellular extracts from $CSB^{+/+}$, $CSB^{+/-}$, and $CSB^{-/-}$ mouse fibroblasts. The wild-type mouse CSB protein was detected with an antibody raised against the C-terminal domain of the human CSB protein.

agreement with the absence of wild-type *CSB* mRNA, the 160 kDa wild-type CSB protein could not be detected in extracts from $CSB^{-/-}$ fibroblasts, as shown by Western blot analysis using antibodies raised against the C-terminal domain of the human protein (Figure 2B).

CSB-Deficient Mice Display Mild Cockayne Syndrome–Like Symptoms

The Mendelian segregation of the targeted *CSB* allele shows that a deficiency in CSB does not interfere with embryonic or neonatal development. Since in humans the majority of clinical symptoms such as growth retardation and neurological dysfunction become manifest in the first few years after birth (Nance and Berry, 1992), we have carefully watched the mice aging. $CSB^{-/-}$ mice develop normally and are indistinguishable from heterozygous and wild-type littermates. However, a comparison of body weights at the age of 10 weeks reveals a small but highly significant reduction in the body weights of male and a less pronounced tendency to reduced body weights of female $CSB^{-/-}$ mice (Table 1). This finding suggests that growth is slightly affected. $CSB^{-/-}$ male and female mice are fertile, and the length of their reproductive period as well as the litter size is comparable to that of wild-type and heterozygous littermates. Histological examination of testis and ovaries failed to reveal obvious abnormalities.

We also investigated the status of neuromyelination by electron microscopic analysis of perfusion-fixed preparations of the optic and ischiatic nerve of 18-week- and 14-month-old $CSB^{+/+}$ and $CSB^{-/-}$ animals. No apparent differences in overall morphology and thickness of the myelin sheet were observed. This suggests that $CSB^{-/-}$ mice do not exhibit gross neurological abberations, but does not exclude minor abnormalities. Interestingly, as a potential indication of neurodysfunction, we found that after 6 months of age a significant fraction

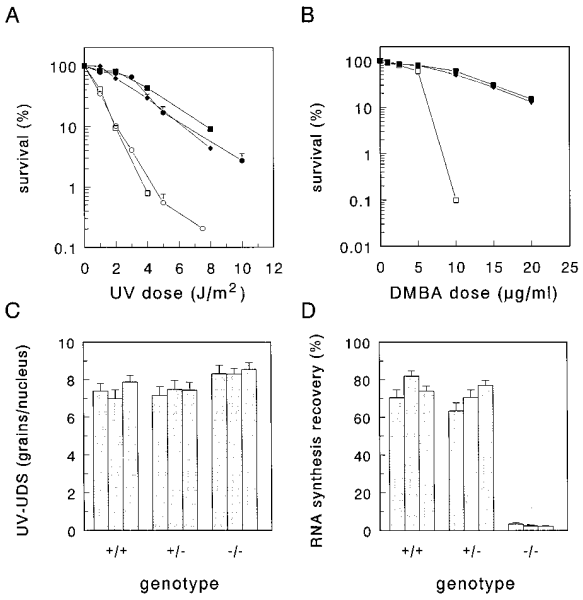

Figure 3. Repair Characteristics of CSB-Deficient Mouse Embryonic Fibroblasts

(A) UV survival curves of a $CSB^{+/+}$ (closed squares), $CSB^{+/-}$ (diamonds), and $CSB^{-/-}$ (open squares) fibroblast line. For each genotype, identical results were obtained with two other lines (data not shown). For comparison, UV survival curves of normal (closed circles) and CS1AN (open circles) human fibroblasts are included. For details see Experimental Procedures.

(B) DMBA survival curves of a $CSB^{+/+}$ (closed squares), $CSB^{+/-}$ (diamonds), and $CSB^{-/-}$ (open squares) fibroblast line. Cells were grown for 3 hr in the presence of the indicated doses of DMBA. For details see Experimental Procedures.

(C) Global genome repair (UDS) in $CSB^{+/+}$, $CSB^{+/-}$, and $CSB^{-/-}$ fibroblasts (three independent lines per genotype). Cells were irradiated with 16 J/m^2 254 nm UV and labeled with [methyl-^{3}H]thymidine. Incorporation of radioactivity was measured by autoradiography and grain counting (average of 50 nuclei per cell line; short lines represent the standard error of the mean).

(D) RNA synthesis recovery of $CSB^{+/+}$, $CSB^{+/-}$, and $CSB^{-/-}$ fibroblasts (three independent lines per genotype) 16 hr after exposure to 10 J/m^2 254 nm UV. RNA synthesis was measured by grain counting (average of 50 nuclei per cell line) following a 1 hr pulse labeling with [^{3}H]uridine. RNA synthesis recovery is expressed as the quotient of the number of grains over UV-exposed and nonexposed nuclei (percentage; short lines represent the standard error of the mean).

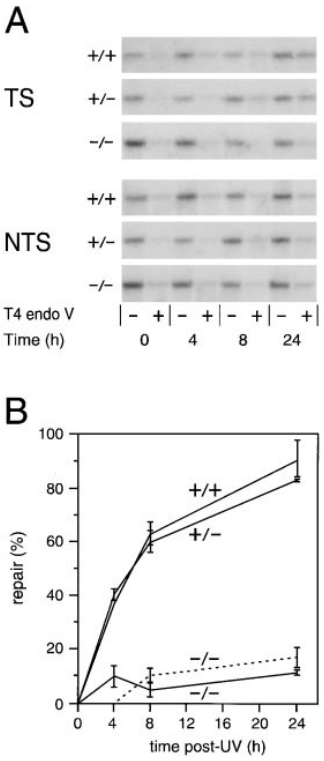

Figure 4. Defective Transcription-Coupled Repair of the *p53* Gene in CSB-Deficient Mouse Embryonic Fibroblasts

$CSB^{+/+}$, $CSB^{+/-}$, and $CSB^{-/-}$ fibroblasts were irradiated with 10 J/m^2 254 nm UV and allowed to repair for the indicated times. Genomic DNA was EcoRI digested, treated or mock-treated with T4 endonuclease V (indicated by + or −), and electrophoresed under denaturing conditions. Southern blot analysis was performed using probes specific for the transcribed (TS) or nontranscribed (NTS) strand of the *p53* gene. After measurement of the amount of radioactivity (four independent gels), the percentage of repair was calculated.

(A) Representative autoradiographs.

(B) Graphical presentation of strand-specific repair of the *p53* gene in the three different genotypes. Solid lines, TS; dashed lines, NTS (average of four blots; vertical lines represent the standard error of the mean).

of male and female $CSB^{-/-}$ mice started to develop a stereotypic hyperactive behavior known as circling or waltzing. Because circling is associated with inner ear defects, this finding is highly suggestive of the development of deafness in $CSB^{-/-}$ mice. The oldest $CSB^{-/-}$ animals are now 22 months old and have not developed other overt CS features such as tremors or limb ataxia.

To examine the presence of minor neurologic abnormalities in $CSB^{-/-}$ mice, several behavioral tests were performed on 18-week-old mice (see Table 1). Gross behavioral abnormalities such as hyperactivity or ataxia were examined using an open-field exploratory test. Although $CSB^{-/-}$ mice showed normal behavior, they were significantly less active, especially in the first 30 s of the test. Apparently, $CSB^{-/-}$ mice require more time to adapt to a new environment. Hind foot pattern analysis did not reveal any gait abnormalities. However, when motor coordination and balance were tested in a Rotarod task test, it appeared that $CSB^{-/-}$ mice had more difficulties remaining on the rotating cylinder than heterozygous and wild-type mice. The behavioral and motor coordination tests are indicative of the presence of minor neurologic dysfunction in $CSB^{-/-}$ mice. Taken together, our data show that, in contrast to patients with CS, CSB-deficient mice develop only a mild CS-like phenotype.

CSB-Deficient Mice Are Defective in Transcription-Coupled Repair

To confirm that targeted disruption of the mouse *CSB* gene resulted in defective transcription-coupled NER, various DNA repair parameters were analyzed in primary mouse embryonic fibroblasts. First, the cellular survival after exposure to increasing UV doses was determined. Figure 3A shows that fibroblasts of CS-B patient CS1AN and $CSB^{-/-}$ mice were equally UV-sensitive. As expected for an autosomal recessive defect, UV-survival of $CSB^{+/-}$ fibroblasts was within the wild-type range. Similarly, $CSB^{-/-}$ fibroblasts showed decreased survival when

Table 1. In Vivo Analysis of *CSB* Genotypes

Parameter	Sex	Age (weeks)	+/+[a] +/−	−/−	p
Body weight (g)	♂	10	29.8 ± 0.4 (104)	26.3 ± 0.6 (40)	<0.00001
	♀	10	24.5 ± 0.5 (65)	23.2 ± 0.6 (33)	0.122
Fertility	♂ + ♀	6–60	Normal	Normal	
Gait pattern	♂ + ♀	18	Normal	Normal	
Rotarod, latency to fall (s)	♂	18	182 ± 33 (17)	69 ± 37 (9)	0.046
Locomotory activity (squares/3 min)	♂	18	221 ± 10 (18)	176 ± 17 (9)	0.042
Locomotory activity (squares/30 s)	♂	18	35.5 ± 3.2 (18)	20.7 ± 3.1 (9)	0.0075
Circling (waltzing) behavior	♂ + ♀[b]	>26	1.8% (109)	16% (69)	0.00037
Skin cancer proneness					
UV					
Latency time (T_{50}, days)	♂ + ♀[b]		290	233	0.0004
Yield (tumors/animal)			0.18 (28)	1.3 (13)	<0.00001
DMBA					
Latency time (T_{50}, days)	♀		357	257	0.15
Yield (tumors/animal)			0.31 (19)	1.1 (10)	0.012

Values are the mean ± SEM; number of mice tested are given in parentheses.
[a]No significant difference observed between +/+ and +/−.
[b]No significant difference observed between ♂ and ♀.

grown in medium containing DMBA, a chemical carcinogen that forms bulky DNA adducts (Figure 3B). The global genome repair capacity of $CSB^{-/-}$ fibroblasts was examined using the UV-induced repair synthesis assay (unscheduled DNA synthesis [UDS]). As is evident from Figure 3C, the wild-type UDS levels observed in $CSB^{-/-}$ cells indicate that they are global genome repair–proficient. A third characteristic of CS cells is their inability to recover RNA synthesis after UV exposure (Mayne and Lehmann, 1982). Figure 3D shows that 16 hr after UV treatment, $CSB^{-/-}$ fibroblasts had not resumed transcription, while $CSB^{+/-}$ and $CSB^{+/+}$ cells showed RNA synthesis restored to near normal levels. These data strongly suggest that, analogous to human CS cells, CSB-deficient mouse fibroblasts are impaired in TCR.

The hallmark of CS is the inability to focus repair on the transcribed strand of active genes to allow resumption of transcription elongation by RNA polymerases stalled at lesions. This feature was investigated by determining the rate of repair of UV-induced lesions in both strands of the active *p53* gene and the inactive c-*mos* gene. For CPDs, wild-type mouse fibroblasts displayed the strong strand bias characteristic of repair of active genes (Figures 4A and 4B): in the *p53* gene, lesions are rapidly removed from the transcribed strand by TCR, whereas the nontranscribed strand is slowly repaired by the global genome repair pathway. However, in $CSB^{-/-}$ cells the transcribed strand was repaired as inefficiently as the nontranscribed strand (very low levels of repair at 24 hr). In wild-type as well as in CSB-deficient mouse fibroblasts, the transcribed and nontranscribed strands of the inactive c-*mos* gene are repaired at low rates typical for global genome repair (data not shown). From these data we conclude that the CSB-deficient mouse is specifically defective in TCR and accordingly forms a bona fide animal model for the repair characteristics of human CS.

CSB-Deficient Mice Are Photosensitive and Skin Cancer Prone

CS patients have photosensitive skin but remarkably, despite their NER defect, have not been reported to develop skin cancer. The photosensitivity of $CSB^{-/-}$ mice was tested by exposing the shaven dorsal skin of wild-type, heterozygous, and homozygous mutant littermates to UV-B light at environmentally relevant dose rates ranging from 100 to 1000 J/m²/day for 4 consecutive days. At all doses tested, $CSB^{-/-}$ mice developed mild to severe erythema within 5 days (Figure 5A). At the highest dose, $CSB^{-/-}$ mice avoided contact with daylight by keeping their eyes closed. This photophobia disappeared a few days after treatment. Histological analysis of skin sections of $CSB^{+/+}$ and $CSB^{-/-}$ mice revealed epidermal hyperplasia, consisting of both an increase in the number of viable cell layers (acanthosis) and cornified layers (hyperkeratosis) in the latter (Figures 5B and 5C). Erythema and hyperplasia were not observed either in the UV-exposed skin of heterozygous mice or in the unexposed skin of $CSB^{-/-}$ mice (data not shown).

With regard to the remarkable absence of a clear predisposition to UV-induced skin cancer, it was important to investigate this parameter in the CSB-deficient mouse model. To this end, mice (14 animals per genotype) were chronically exposed to low daily doses of UV light. After 10 weeks (cumulative UV-B dose ≈ 10 kJ/m²), marked macroscopic changes started to develop exclusively on the skin and in the eyes of $CSB^{-/-}$ mice. UV-exposed areas of the skin showed redness and scaling, and scratching marks were indicative of pruritus. Corneal opacity and bulging were observed in the eyes (data not shown). As the experiment continued, cutaneous scaling (Figure 5D), pruritus, and eye lesions increased in severity. Histopathological analysis of killed mice demonstrated acanthosis and parakeratosis in the chronically UV-exposed skin of $CSB^{-/-}$ mice (Figure 5E). The eye malformations were recognized as corneal intraepithelial neoplasias (Bowenoid lesions), which in some cases showed progression into squamous cell carcinomas (data not shown). Histological changes were not observed in the skin and eyes of UV-exposed wild-type and heterozygous animals. After 23 weeks, $CSB^{-/-}$ mice started to develop multiple skin tumors in UV-exposed areas. From weeks 27 and 34 onward, single

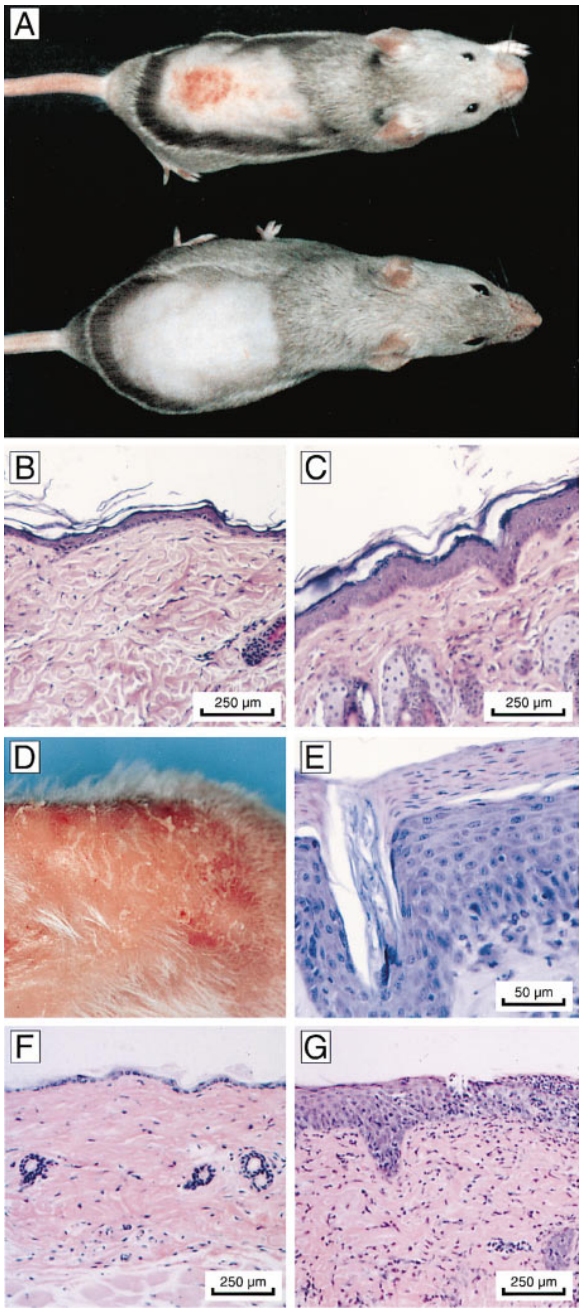

Figure 5. Acute and Chronic Effects in the Skin of CSB-Deficient Mice after Exposure to UV or DMBA

(A) UV-induced erythema in the skin of $CSB^{-/-}$ mice. Shaven animals were exposed to UV-B (1000 J/m^2/day) for 4 consecutive days (photographs taken 1 week after the first exposure). (Top) $CSB^{-/-}$ male mouse (note reduced size). (Bottom) Wild-type male mouse.

(B and C) Skin sections of shaven $CSB^{+/+}$ (B) and $CSB^{-/-}$ (C) mice after exposure to UV-B (200 J/m^2/day) for 4 consecutive days. The wild-type skin appears normal. The CSB-deficient skin shows hyperplasia (acanthosis and hyperkeratosis).

(D and E) Skin of a $CSB^{-/-}$ mouse after chronic exposure to UV-B (cumulative dose 30 kJ/m^2). Macroscopic changes include redness and scaling (D), and histologic changes include acanthosis and parakeratosis (E).

(F and G) Skin sections of shaven $CSB^{+/+}$ (F) and $CSB^{-/-}$ (G) mice after three weekly treatments with 5 μg DMBA. The wild-type skin shows normal morphology. The CSB-deficient skin demonstrates strong hyperplasia (acanthosis).

tumors appeared in wild-type and heterozygous mice, respectively. The time course of tumor formation and tumor yield are shown in Figure 6A and 6B. Because of the severity of pruritus and eye lesions, tumor-bearing $CSB^{-/-}$ mice were withdrawn from the experiment a few weeks after detection of the first tumor, probably resulting in underestimation of the tumor yield. All tumors were histologically classified as squamous cell carcinomas (Figure 6C). The significantly decreased latency time and increased tumor yield (Table 1) indicate that CSB-deficient mice are more susceptible to UV carcinogenesis than wild-type and heterozygous mice.

The CSB-deficient mouse model allowed us to test whether CS is associated with increased susceptibility to chemically induced carcinogenesis. We have shown that $CSB^{-/-}$ mouse fibroblasts are sensitive to the model carcinogen DMBA (Figure 3B). Mice (10 animals per genotype) were subjected to a complete carcinogenesis protocol comprising 18 weekly applications with a low dose (5 μg) of DMBA on the shaven dorsal skin. After 3 treatments, an inflammatory reaction with crust formation and loss of hair growth at the application area was observed in $CSB^{-/-}$ mice only. Similar effects were observed in the skin of $XPA^{-/-}$ mice (de Vries et al., 1995), used in this experiment as a control for the effectiveness of the DMBA dose (data not shown). Histopathological changes include strong hyperplasia (acanthosis) and spongiosis with necrosis, not present in the skin of treated wild-type and heterozygous mice (Figures 5F and 5G). After 14 weeks, $CSB^{-/-}$ as well as (control) $XPA^{-/-}$ mice started to develop skin tumors, whereas single tumors appeared in heterozygous and wild-type mice after 24 and 27 weeks, respectively (Figures 6D and 6E). Tumors in $CSB^{-/-}$ mice were histologically identified as papillomas (Figure 6F) and squamous cell carcinomas (similar to the tumor shown in Figure 6C) at a ratio of 1:3. All tumors in heterozygous and wild-type mice were squamous cell carcinomas. Although we could not demonstrate a statistically significant decrease in the latency time of DMBA-induced tumor formation in $CSB^{-/-}$ mice, the observed significant increase in tumor yield suggests that CSB-deficient mice are also more susceptible to chemically induced skin cancer than wild-type and heterozygous mice (Table 1).

Discussion

CSB-Deficient Mice as a Model for the Transcription-Coupled Repair Defect in Cockayne Syndrome

We have generated a mouse mutant with a selective defect in TCR to establish an experimental animal model for the NER disorder CS. The *CSB/ERCC6* gene was interrupted by insertion of a premature stopcodon, skipping all identified functional domains and closely mimicking the K_{337}→stop mutation in a CS-B patient (Troelstra et al., 1992). Mutant mice express reduced levels of the *CSB–neo* fusion transcript and are unable to produce the wild-type protein. We have shown that disruption of mouse *CSB* results in a clear DNA repair defect very similar to the human syndrome: CSB-deficient mouse fibroblasts display UV sensitivity, defective resumption of transcription after UV exposure, normal

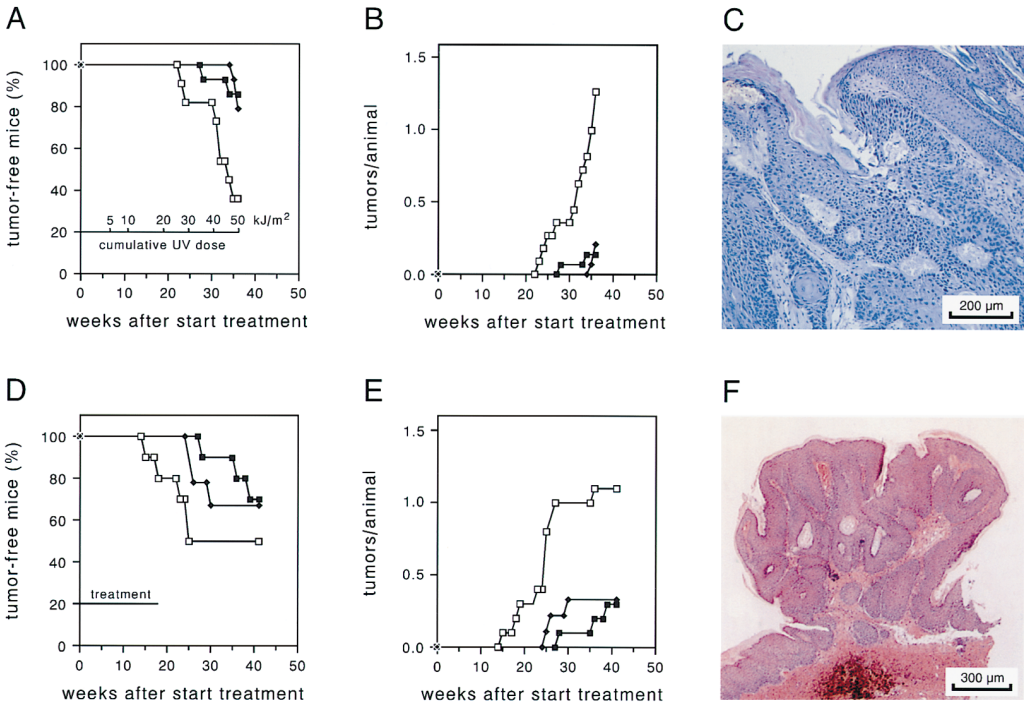

Figure 6. Tumor Development on the Skin of CSB-Deficient Mice after Exposure to UV-B or DMBA

Shaven $CSB^{+/+}$, $CSB^{+/-}$, and $CSB^{-/-}$ mice were subjected to an incremental-dose UV-B carcinogenesis protocol or a complete DMBA carcinogenesis protocol. For details see Experimental Procedures. For statistical data on latency times and tumor yield see Table 1. Closed squares, $CSB^{+/+}$; diamonds, $CSB^{+/-}$; open squares, $CSB^{-/-}$.

(A) Time course of skin tumor formation during chronic exposure to UV-B. The cumulative UV-dose during the experiment is indicated.

(B) Skin tumor yield during chronic exposure to UV-B.

(C) Histological examination of UV-induced skin tumors in $CSB^{-/-}$ mice. Shown is a typical example of a well-differentiated squamous cell carcinoma. Other tumor types were not observed.

(D) Time course of skin tumor formation after exposure to DMBA.

(E) Skin tumor yield after treatment with DMBA.

(F) Histological examination of DMBA-induced skin tumors in $CSB^{-/-}$. Shown is a typical example of a papilloma, found in about 25% of the cases. The remainder of tumors were squamous cell carcinomas similar to the one shown in (C).

global genome repair, and a complete loss of TCR of CPDs in the transcribed strand of an active gene. Thus, the role of CSB in repair is the same in rodents and primates, and CSB-deficient mice constitute a valid animal model for the TCR defect of the human disorder.

The basic NER reaction is strikingly conserved in eukaryotic evolution. Recently, the Saccharomyces cerevisiae homolog of *CSB*, *RAD26*, was cloned. In analogy with human CS-B, a *rad26*Δ mutation also affects TCR of CPDs. Surprisingly, the *rad26* mutant is not UV-sensitive, probably because in lower eukaryotes the efficient global genome repair is the major determinant of UV resistance, and *rad26* mutants still exhibit some residual TCR (van Gool et al., 1994). Moreover, introduction of a global genome repair defect on top of a TCR deficiency (*rad7/rad26* and *rad16/rad26* double mutants) did not further reduce the residual repair of the transcribed strand of active genes, while, as expected, the nontranscribed strand was no longer repaired (Verhage et al., 1996). Apparently, yeast cells also possess a *RAD26*-independent transcription-coupled mechanism for repair of CPDs. It is presently unknown whether such a (CSB-independent) backup system exists in mammalian cells as well. However, our finding that in CSB-deficient mice, repair of the transcribed strand follows the rodent-specific very inefficient CPD removal by the global genome repair system suggests that mammalian cells lack an additional CSB-independent TCR mechanism. Thus, CSB constitutes an indispensable component of TCR, and in CS-B patients the slow but significant CPD repair seen in the transcribed strand is likely derived from the global genome NER pathway, which is more efficient in humans than in mice.

CSB-Deficient Mice as a Model for the Clinical Features of Cockayne Syndrome

A general hallmark of NER disorders is sun sensitivity. Acute effects such as photophobia and development of erythema and hyperplasia in exposed areas of the skin are clear signs that CSB-deficient mice resemble CS patients in this parameter. In addition, chronic UV exposure resulted in redness and scaling of the skin, pruritus, corneal opacities, and severe ulceration of the eyes. The parakeratosis observed in the skin suggests that terminal epidermal differentiation is disturbed in chronically exposed CSB-deficient mice. Except for the photophobia and parakeratosis, similar findings were reported

for UV-exposed XPA- and XPC-deficient mice (de Vries et al., 1995; Nakane et al., 1995; Sands et al., 1995).

In addition to cutaneous photosensitivity, diagnostic criteria for CS involve poor growth, impaired sexual development, and neurologic anomalies, including psychomotor problems, hearing loss, and ophthalmologic abnormalities. The reported average age of death is close to 12 years (Nance and Berry, 1992). Surprisingly, CSB-deficient mice do not show pronounced symptoms for these aspects of the CS phenotype. A reduced life span, reproductive problems, and severe neurologic dysfunctioning are not observed. Nevertheless, the lower body weight of male mice, the waltzing behavior, and the poorer performance of CSB-deficient mice in open-field and motor coordination tests are suggestive of the presence of a minor growth disturbance, deafness, and mild neurological dysfunctioning. Moreover, very recently we obtained evidence that CSB-deficient mice develop age-dependent blindness at a high incidence (unpublished data). None of the latter features is exhibited by XPA-deficient mice that carry a total NER defect (de Vries et al., 1995). These extra symptoms strongly argue for an additional function of the mouse CSB protein outside the context of NER.

Previously, we put forward the ''transcription-repair syndrome'' hypothesis to account for the extra CS and TTD features of mutations in the XPB and XPD subunits of the dual-functioning transcription/repair factor TFIIH (Schaeffer et al., 1993, 1994; Vermeulen et al., 1994b). This clinical correspondence between CS and TFIIH mutations suggests a link between the CS proteins and basal transcription (Hoeijmakers et al., 1996). The CS features in CSB-deficient mice are less pronounced than those in CS individuals. A major difference is the time factor: CS characteristics in patients develop over the course of years, which is an order of magnitude longer than in mice. A possible explanation for the origin of the CS symptoms and the link with TFIIH transcription function is time-dependent accumulation of DNA damage in cells of specific tissues. Such lesions likely trap transcription components: CSB-dependent TCR might involve their release (see also van Oosterwijk et al., 1996). In the absence of CSB, protein transcription in these cells may become crippled. In support of a link between accumulation of DNA damage and CS features, we recently observed that further impairment of NER by crossing CSB mice with XPA- or XPC-deficient mice leads to dramatic worsening of the CS symptoms (our unpublished findings). This observation underscores a direct relationship between NER capacity and the severity of CS hallmarks.

Cockayne Syndrome and Cancer Predisposition

One of the most important and puzzling disparities between CS and XP is the difference in cancer incidence. XP-A patients carrying total NER paralysis are highly cancer prone. In addition, a defect in the *XPC* gene, which selectively inactivates global genome repair, strongly predisposes to skin cancer. The absence of such a clear oncogenic predisposition in human CS suggests that, at least in humans, global genome repair rather than TCR constitutes the main determinant of the prevention of UV-induced mutagenic and carcinogenic events. An alternative or additional explanation for the absence of cancer predisposition in CS is that persistent transcription-blocking lesions due to the TCR defect may provide an efficient trigger for programmed cell death, eliminating potentially oncogenic cells and explaining the high UV sensitivity of CS patients (Ljungman and Zhang, 1996).

In contrast to the lack of cancer proneness in human CS, our UV and DMBA carcinogenesis experiments have uncovered a clear skin cancer predisposition in CSB-deficient mice. Thus, global genome repair on its own is not capable of preventing mutagenic events. TCR certainly contributes to the removal of mutagenic UV-induced lesions as well as DMBA-induced lesions, which apparently also form a substrate for this NER pathway. To assess the relative contribution of defects in the different NER subpathways to cancer susceptibility, it is necessary to compare XPA-, XPC- and CSB-deficient mice with the same genetic background and protocol of UV exposure (study in progress). A tentative comparison is made in Table 2 for XPA- and CSB-deficient mice using the same irradiation setup. Although variation due to differences in genetic background is not excluded, these data suggest that CSB-deficient mice require a higher cumulative dose and longer latency time before they develop skin cancer. This would be consistent with the notion that XPA-deficient mice carry a defect in both NER subpathways and thus reveal the combined contribution of TCR and global genome repair to cancer susceptibility. Another implication of the findings above is that elimination of precancerous cells by apoptosis triggered by transcription-blocking lesions is apparently insufficient to compensate for the increased mutagenesis in CSB-deficient mice.

The notion that rodent mutants for XPA (de Vries et al, 1995; Nakane et al., 1995), XPC (Sands et al., 1995), and CSB (this study) are all associated with cancer predisposition suggests that CS may not be very different from XP. The intriguing question of why skin cancer has not been observed in human CS can be answered in several ways. First, an important difference between rodent and human NER is the more potent global genome repair of CPD lesions in humans, removing eventually most CPDs from both strands. In mice the relative impact of TCR on mutagenesis is much greater because of inefficient backup by global genome repair. This difference implies that CS patients have a lower risk of skin cancer than CS mice. Moreover, on the basis of the comparison of rodent XP-A and CS-B, it is thought that human CS would also demonstrate a longer latency

Table 2. UV-Induced Tumorigenesis in CSB- and XPA-Deficient Mice

	$CSB^{-/-}$ [a]	$XPA^{-/-}$ [b]
Genetic background	FVB/Ola129	C57BL6/J/Ola129
Tumor bearing animals (%)	65	75
Onset of tumors (weeks)	23–36	15–23
Cumulative UV dose (kJ/m^2)	50	22

[a]This study.
[b]de Vries et al. (1995).

time for skin tumor induction than the average 8 years observed in XP. In addition, CS patients are severely affected, need frequent hospitalization and indoor protection, and have a short average lifespan (approximately 12 years). Consequently, CS patients may never receive the relevant exposure nor survive the latency period required to develop skin cancer.

Experimental Procedures

Disruption of *CSB* in Mouse ES Cells

Isogenic mouse genomic DNA was derived from an Ola129 ES cell–derived cosmid library (kindly provided by Dr. N. Galjart, Erasmus University) probed with human *CSB* cDNA sequences. The targeting construct pG7CSBko1 (see Figure 1A), containing exon 5 of the *CSB* gene, was generated from a 7.0 kb NcoI–BamHI fragment subcloned in pGEM7. First, NcoI and BamHI sites were substituted for NotI sites by mung bean nuclease treatment and insertion of a NotI linker. Next, the XhoI–BglII fragment was swapped for a similar fragment carrying ochre MURFI linker 5′-TTAAGTTAACTTAA-3′ (containing a diagnostic HpaI site) in the mung bean nuclease-treated PstI site. Finally, exon 5 was interrupted with a floxed (TK promoter–driven) neomycin-resistance gene, cloned in sense orientation in the unique NarI site with the use of ClaI linkers. The floxed *neo* resistance cassette was generated from pGH-1 and pGEM-30 (kindly provided by Dr. W. Gu, University of Cologne) via deletion of the BamHI fragment (herpes simplex virus thymidine kinase gene) from pGH-1, addition of a SalI-linker, and subsequent insertion of the SalI–XhoI *loxP* fragment of pGEM-30.

The Ola129-derived ES cell line E14 (kindly provided by Dr. A. Berns, The Netherlands Cancer Institute) was maintained on gelatin-coated dishes in 60% buffalo rat liver cell conditioned DMEM/40% fresh DMEM medium, supplemented with 15% fetal calf serum, 0.1 mM nonessential amino acids, 2 mM glutamine, 50 μg/ml penicillin and streptomycin, 1000 U/ml leukemia inhibitory factor (all components purchased from GIBCO), and 0.1 mM 2-mercaptoethanol.

The 8.8 kb NotI insert (15 μg) from clone pG7CSBko1 was transfected into E14 cells (1×10^7 cells in 400 μl PBS) by electroporation for 10 ms at 1200 μF and 117 V, using a Progenetor II Gene Pulser (Hoeffer). Electroporated cells were reseeded onto 10 cm dishes and subjected to neomycin selection by addition of 200 μg/ml G418 (Geneticin, GIBCO) the following day. After 9 days, G418-resistant colonies were randomly picked and expanded in 24-well dishes. Duplicate dishes were used for cryopreservation and genotyping (Southern blot analysis), respectively.

Generation of Mutant Mice and Fibroblasts

Gene-targeted ES cells (two independent clones) were injected into C57BL/6J blastocysts by standard procedures (Bradley, 1987). Chimeric male mice were mated with FVB females, and transmission of E14-derived germ cells was recognized on the basis of the gray coat color of the offspring. Heterozygous male and female mice were interbred to generate *CSB*$^{+/+}$, *CSB*$^{+/-}$, *and CSB*$^{-/-}$ mice.

Primary mouse embryonic fibroblasts (three independent lines/genotype) were isolated from day 13.5 embryos obtained from matings between *CSB*$^{+/-}$ mice (F1). Cells were grown in DMEM medium, supplemented with 10% fetal calf serum, 2 mM glutamine, and 50 μg/ml penicillin and streptomycin.

DNA, RNA, and Protein Analysis

Analysis of ES cell, tail, or embryonic tissue DNA was performed by Southern blot analysis. For standard genotyping, NcoI-digested DNA was probed with a 0.8 kb BamHI–NcoI intron 5 fragment, located downstream of the targeting construct. The presence of the ochre MURFI linker was detected by the appearance of an additional HpaI site in HpaI/BglII-digested DNA probed with the exon 5 fragment. The selectable marker was detected using a PCR probe spanning the coding region of the neomycin-resistance gene.

RNA was examined by combined RT-PCR/restriction analysis. Randomly primed fibroblast cDNA was synthesized from mRNA isolated with a Quick prep mRNA isolation kit (Pharmacia). After PCR amplification using primer set FP/RP (see Figure 1A), wild-type and mutant PCR products (664 and 674 bp, respectively) were distinguished by digestion with HpaI or PstI.

Western blot analysis of mouse CSB protein was performed on fibroblast extracts obtained by sonication (5×10^6 cells in 300 μl PBS). Twenty micrograms of total cellular protein was separated on a 7% SDS-polyacrylamide gel and blotted to nitrocellulose. Wild-type mouse CSB protein was visualized using a rabbit polyclonal antibody raised against the C-terminal part of human CSB protein and an anti-rabbit IgG/alkaline phosphatase detection system.

DNA Repair Assays

UV sensitivity was determined as described (Sijbers et al., 1996). Sparsely seeded Petri dish cultures were exposed to different doses of UV (254 nm, Philips TUV lamp). After 4 days, the number of proliferating cells was estimated from the amount of radioactivity incorporated during a 2 hr pulse with [^{3}H]thymidine. Cell survival was expressed as the percentage of radioactivity in exposed cells in relation to the radioactivity in untreated cells.

The sensitivity of embryonic fibroblasts to the chemical carcinogen 7,12-di-methylbenz[*a*]-anthracene (DMBA) was determined as described by de Vries et al. (1995).

UV-induced global genome repair was assayed using the UDS method described by Vermeulen et al. (1994a). In brief, coverslip-grown cells were exposed to 16 J/m^2 of 254 nm UV light and labeled with [^{3}H]thymidine. Repair capacity was quantified by grain counting after autoradiography.

RNA synthesis recovery was measured according to Mayne and Lehmann (1982). In short, coverslip-grown cells were exposed to 10 J/m^2 of 254 nm UV light, allowed to recover for 16 hr, labeled with [^{3}H]uridine, and processed for autoradiography. The relative rate of RNA synthesis was expressed as G_{UV}/G_C (percentage), where G_{UV} and G_C represent the number of grains over UV-exposed and nonexposed nuclei, respectively.

Strand-specific removal of UV-induced CPDs from a 16 kb EcoRI fragment of the active *p53* gene and a 22 kb BamHI fragment of the inactive c-*mos* gene was analyzed as described by Bohr et al. (1985). Embryonic fibroblasts were grown to confluency and maintained for 3 days in medium containing heat-inactivated serum. After exposure to UV (10 J/m^2, 254 nm), cells were allowed to repair for 0, 4, 8, or 24 hr and were lysed in 150 mM NaCl, 10 mM Tris-HCl (pH 8.0), 1 mM EDTA, 0.5% SDS, and 100 μg/ml proteinase K (16 hr, 37°C). Genomic DNA was digested with EcoRI or BamHI and treated or mock-treated with T4 endonuclease V, electrophoresed on denaturing agarose gels, and transferred to Hybond N$^+$ membranes. After hybridization with linear PCR–derived strand-specific probes (Ruven et al., 1994), membranes were scanned using a PhosphorImager (Molecular Dynamics). Repair of CPDs was calculated by comparing the amount of radioactivity in the T4 endonuclease V–treated versus mock-treated fragments.

Behavioral and Neuromotor Activity Tests

In each experiment, age- and sex-matched mice were tested in randomized order between 10:00 a.m. and 4:00 p.m. To eliminate olfactory cues, equipment was cleaned with alcohol and dried between each session.

Open-field exploratory behavior was tested in a gray plastic box ($50 \times 30 \times 20$ cm). The bottom was covered with a transparent plastic-coated sheet of paper with a 5×5 cm grid pattern. Each session lasted 3 min, and movements of the mice were videotaped and later analyzed. Locomotory activity was defined as the number of squares entered by the mouse with both of its forepaws.

Motor coordination was tested with a locally manufactured Rotarod apparatus consisting of a gritted plastic rod (3.5 cm diameter) with a 10 cm compartment made of two plastic discs (25 cm diameter). The rod was rotated by a motor at defined speeds, and the time each mouse remained on the rod was measured.

Hind foot patterns were analyzed by dipping the hind legs of the mice in India ink and allowing them to walk on a sheet of white paper. The length of steps and the base between the hind feet was measured.

UV and Chemically Induced Skin Effects and Carcinogenesis

Acute effects in the skin of shaven *CSB*$^{+/+}$, *CSB*$^{+/-}$, and *CSB*$^{-/-}$ mice following exposure to UV (American Philips F40 sun lamps) at doses of 100, 200, 400, 600, and 1000 J/m^2/day (250–400 nm) during 4 consecutive days, or exposure to DMBA (three treatments of 5 μg of DMBA/week) were studied by killing 2 mice per genotype 24 hr after the last treatment. Skin samples were routinely processed (hematoxylin–eosin staining) for histopathologic examination.

UV-induced carcinogenesis was studied by exposing shaven *CSB*$^{+/+}$, *CSB*$^{+/-}$, and *CSB*$^{-/-}$ mice (14 animals per genotype; age 20 weeks) to UV-B light using an incremental-dose protocol starting at 100 J/m^2/day and gradually increasing to 250 J/m^2/day. Timer-controlled American Philips F40 sun lamps were positioned 33 cm above the cage and yielded a dose rate of 8.3 J/m^2/min (250–400 nm) as determined with a UV-B detector (Waldmann, Schwenningen, Germany) calibrated against an Optronics 747 spectroradiometer (Optronics Laboratories, Orlando, FL). Chemically induced carcinogenesis in the mouse skin was tested with DMBA in the complete carcinogenesis protocol described by de Vries et al. (1995). Shaven *CSB*$^{+/+}$, *CSB*$^{+/-}$, and *CSB*$^{-/-}$ female mice (10 animals per genotype; age 8–12 weeks) received 18 weekly applications of 5 μg of DMBA dissolved in 100 μl acetone.

In both protocols, mice were checked twice a week for the development of tumors. Tumor-bearing animals were killed and examined. Skin tumors and suspect UV-exposed eyes were isolated and routinely processed for histopathologic examination.

Received January 6, 1997; revised March 3, 1997.

Acknowledgments

Correspondence should be addressed to G. T. J. v. d. H. We are very grateful to Dr. N. J. Galjart, Dr. A. Berns, and Dr. W. Gu for providing us with materials. C. van Oostrom is kindly acknowledged for performing DMBA survival experiments. We thank Dr. W. Slob for his help in statistical data analysis and M. Kuit for photographic work. This research was supported by The Netherlands Organization for Scientific Research (contract PGN 901-01-093), a fellowship of the Royal Academy of Arts and Sciences of The Netherlands (to G. W.), grants from the Dutch Cancer Society (projects EUR 90-20 and EUR 94-763), and a Human Frontier Science Programme.

References

Aboussekhra, A.M., Biggerstaff, M., Shivji, M.K.K., Vilpo, J.A., Moncollin, V., Produst, V.N., Protic, M., Hübscher, U., Egly, J.M., and Wood, R.D. (1995). Mammalian DNA nucleotide excision repair reconstituted with purified protein components. Cell *80*, 859–868.

Bohr, V.A., Smith, C.A., Okumoto, D.S., and Hanawalt, P.C. (1985). DNA repair in an active gene: removal of pyrimidine dimers from the DHFR gene of CHO cells is much more efficient than in the genome overall. Cell *40*, 359–369.

Bootsma, D., and Hoeijmakers, J.H.J. (1993). Engagement with transcription. Nature *363*, 114–115.

Bootsma, D., Cleaver, J.E., Kraemer, K.H., and Hoeijmakers, J.H.J. (1996). Xeroderma pigmentosum and Cockayne syndrome. In The Metabolic Basis of Inherited Disease, C.R. Scriver, A.L. Beaudet, W.S. Sly, and D. Valle, eds. (New York: McGraw-Hill), in press.

Bradley, A. (1987). Production and analysis of chimeric mice. In Teratocarcinomas and Embryonic Stem Cells: A Practical Approach, E.J. Robertson, ed. (Oxford, UK: IRL Press), pp. 113–151.

de Vries, A., van Oostrom, C.T.M., Hofhuis, F.M.A., Dortant, P.M., Berg, R.J.W., de Gruijl, F.R., Wester, P.W., van Kreijl, C.F., Capel, P.J.A., and van Steeg, H., et al. (1995). Increased susceptibility to ultraviolet-B and carcinogens of mice lacking the DNA excision repair gene XPA. Nature *377*, 169–173.

Friedberg, E.C., Walker, G.C., and Siede, W. (1995). DNA Repair and Mutagenesis (Washington, D.C: ASM Press).

Hanawalt, P.C. (1994). Transcription-coupled repair and human disease. Science *266*, 1957–1958.

Hanawalt, P.C., Donahue, B.A., and Sweder, K.S. (1994). Collision or collusion? Curr. Biol. *4*, 518–521.

Henning, K.A., Li, L., Iyer, N., McDaniel, L.D., Reagan, M.S., Legerski, R., Schultz, R.A., Stefanini, M., Lehmann, A.R., and Mayne, L.V., et al. (1995). The Cockayne syndrome group A gene encodes a WD repeat protein that interacts with CSB protein and a subunit of RNA polymerase II TFIIH. Cell *82*, 555–564.

Hoeijmakers, J.H.J. (1994) Human nucleotide excision repair syndromes: molecular clues to unexpected intricacies. Eur. J. Cancer *30A*, 1912–1921.

Hoeijmakers, J.H.J., Egly, J.M., and Vermeulen, W. (1996). TFIIH: a key component in multiple DNA transactions. Curr. Opin. Genet. Dev. *6*, 26–33.

Itin, P.H., and Pittelkow, M.R. (1990). Trichothiodystrophy: Review of sulfur-deficient brittle hair syndromes and association with the ectodermal dysplasias. J. Am. Acad. Dermatol. *22*, 705–717.

Ljungman M., and Zhang, F. (1996). Blockage of RNA polymerase as a possible trigger for U. V. light-induced apoptosis. Oncogene *13*, 823–831.

Mayne, L.V., and Lehmann, A.R. (1982). Failure of RNA synthesis to recover after UV irradiation: an early defect in cells from individuals with Cockayne's syndrome and xeroderma pigmentosum. Cancer Res. *42*, 1473–1478.

Mellon, I., Spivak, G., and Hanawalt, P.C. (1987). Selective removal of transcription-blocking DNA damage from the transcribed strand of the mammalian DHFR gene. Cell *51*, 241–249.

Nakane, H., Takeuchi, S., Yuba, S., Saijo, M., Nakatsu, Y., Ishikawa, T., Hirota, S., Kitamura, Y., Kato, Y., and Tsunoda, Y., et al. (1995). High incidence of ultraviolet-B- or chemical-carcinogen-induced skin tumors in mice lacking the xeroderma pigmentosum group A gene. Nature *377*, 165–168.

Nance, M.A., and Berry, S.A. (1992). Cockayne syndrome. Review of 140 cases. Am. J. Med. Genet. *42*, 68–84.

Peterson, C.L. (1996). Multiple SWItches to turn on chromatin? Curr. Opin. Genet. Dev. *6*, 171–175.

Ruven, H.J.T., Seelen, C.M.J., Lohman, P.H.M., Mullenders, L.H.F., and van Zeeland, A.A. (1994). Efficient synthesis of 32P-labeled single-stranded probes using linear PCR: application of the method for analysis of strand-specific DNA repair. Mutat. Res. *315*, 189–195.

Sands, A.T., Abuin, A., Sanchez, A., Conti, C.J., and Bradley, A. (1995). High susceptibility to ultraviolet-induced carcinogenesis in mice lacking *XPC*. Nature *377*, 162–165.

Schaeffer, L., Roy, R., Humbert, S., Moncollin, V., Vermeulen, W., Hoeijmakers, J.H.J., Chambon, P., and Egly, J.M. (1993). DNA repair helicase: a component of BTF2 (TFIIH) transcription factor. Science *260*, 58–63.

Schaeffer, L., Moncollin, V., Roy, R., Staub, A., Mezzina, M., Sarasin, A., Weeda, G., Hoeijmakers, J.H.J., and Egly, J.M. (1994). The ERCC2/DNA repair protein is associated with the class II BTF2/TFIIH transcription factor. EMBO J. *13*, 2388–2392.

Sijbers, A.M., de Laat, W.L., Ariza, R.R., Biggerstaff, M., Wei, Y.F., Moggs, J.G., Carter, K.C., Shell, B.K., Evans, E., and de Jong, M.C., et al. (1996). Xeroderma pigmentosum group F caused by a defect in a structure-specific DNA repair endonuclease. Cell *86*, 811–822.

Troelstra, C., van Gool, A., de Wit, J., Vermeulen, W., Bootsma, D., and Hoeijmakers, J.H.J. (1992). ERCC6, a member of a subfamily of putative helicases, is involved in Cockayne's syndrome and preferential repair of active genes. Cell *71*, 939–953.

van Gool, A.J., Verhage, R.A., Swagemakers, S.M.A., van de Putte, P., Brouwer, J., Troelstra, C., Bootsma, D., and Hoeijmakers, J.H.J. (1994). RAD26, the functional S. cerevisiae homolog of the Cockayne syndrome B gene ERCC6. EMBO J. *13*, 5361–5369.

van Hoffen, A., Natarajan, A.T., Mayne, L.V., van Zeeland, A.A., Mullenders, L.H.F., and Venema, J. (1993). Deficient repair of the transcribed strand of active genes in Cockayne's syndrome cells. Nucleic Acids Res. *21*, 5890–5895.

van Oosterwijk, M.F., Versteeg, A., Filon, R., van Zeeland, A.A., and Mullenders, L.H.F. (1996). The sensitivity of Cockayne's syndrome

cells to DNA-damaging agents is not due to defective transcription-coupled repair of active genes. Mol. Cell. Biol. *16*, 4436–4444.

Venema, J., Mullenders, L.H. F., Natarajan, A.T., van Zeeland, A.A., and Mayne, L.V. (1990). The genetic defect in Cockayne syndrome is associated with a defect in repair of UV-induced DNA damage in transcriptionally active DNA. Proc. Natl. Acad. Sci. USA *87*, 4707–4711.

Verhage, R.A., van Gool, A.J., de Groot, N., Hoeijmakers, J.H.J., van de Putte, P., and Brouwer, J. (1996). Double mutants of Saccharomyces cerevisiae with alterations in global genome and transcription-coupled repair. Mol. Cell. Biol. *16*, 496–502.

Vermeulen, W., Scott, R.J., Rodgers, S., Müller, H.J., Cole, J., Arlett, C.F., Kleijer, W.J., Bootsma, D., Hoeijmakers, J.H.J., and Weeda, G. (1994a). Clinical heterogeneity within xeroderma pigmentosum associated with mutations in the DNA repair and transcription gene ERCC3. Am. J. Hum. Genet. *54*, 191–200.

Vermeulen, W., van Vuuren, A.J., Chipoulet, M., Schaeffer, L., Appeldoorn, E., Weeda, G., Jaspers, N.G.J., Priestley, A., Arlett, C.F., and Lehman, A.R., et al. (1994b). Three unusual repair deficiencies associated with transcription factor BTF2 (TFIIH): evidence for the existence of a transcription syndrome. Cold Spring Harb. Symp. Quant. Biol. *59*, 317–329.

Wood, R.D. (1996). DNA repair in eukaryotes. Annu. Rev. Biochem. *65*, 135–167.